Journal of Adhesion Science and Technology

ISSN: 0169-4243 (Print) 1568-5616 (Online) Journal homepage: www.tandfonline.com/journals/tast20

Comparative investigation of composite-metal lap joints with mono-adhesive and thermoplastic-reinforced mixed adhesive at elevated temperatures

Engin Erbayrak, Beril Eker & Murat Colak

JOURNAL OF ADHESION SCIENCE AND TECHNOLOGY
https://doi.org/10.1080/01694243.2026.2658173

Comparative investigation of composite-metal lap joints with mono-adhesive and thermoplastic-reinforced mixed adhesive at elevated temperatures

Engin Erbayrak[a], Beril Eker[b] and Murat Colak[c]

[a]Faculty of & Engineering and Architecture, Istanbul Gelisim University, Istanbul, Türkiye; [b]Science and Technology Application and Research Center, Davutpasa, Yıldız Technical University, Istanbul, Türkiye; [c]Vocational School, Bayburt University, Bayburt, Türkiye

ABSTRACT

This study primarily examines the strength of a single lap joint having a mixed adhesive overlap consisting of a single adhesive and its thermoplastic reinforced state under varying temperatures. In the single lap joint, Titanium-Boron reinforced A356 aluminum was employed as the metal adherend, while plain woven glass fiber-reinforced epoxy (GFRE) was employed as the composite adherend. In the application of the mixed adhesive overlap, the brittle adhesives were employed in the middle section of the lap joint, while the reinforcement of the thermoplastics was employed on the adhesives at both sides of the lap joint. The single lap joints were subjected to tensile tests at 1 mm/min loading rates under room temperature and 120 °C, which is the melting point of the copolyester. In the numerical analysis, the cohesive zone model was applied in order to define the adhesives; however, elastic isotropic and orthotropic material behaviors were employed for the metal and composite adherends, respectively. Eventually, it is determined that the strength of a mixed adhesive lap joint consisting of a single adhesive and its thermoplastic reinforced state is better than a lap joint made with the mono-adhesive alone. Although literature suggests that mixed adhesive overlaps can be formed using at least two different adhesives (one ductile and one brittle), this study demonstrated that a mixed adhesive zone can be created using a single adhesive and thermoplastic reinforcement.

ARTICLE HISTORY
Received 18 February 2026
Revised 1 April 2026
Accepted 6 April 2026

KEYWORDS
Mixed adhesive overlap; metal-composite single lap joint; temperature effect; mixed mode cohesive zone model

1. Introduction

The metal-composite single lap joints are increasing with the applications in areas such as the field of aviation, defense, and automotive industries, etc. Among the other joining methods, the adhesive bonding method is preferred over the other techniques due to factors such as the ability to join different materials, uniform stress distribution, and reduction of weight [1–4]. Among the techniques proposed

CONTACT Engin Erbayrak eerbayrak@gelisim.edu.tr Faculty of & Engineering and Architecture, Istanbul Gelisim University, Istanbul, Türkiye.
Supplemental data for this article can be accessed online at https://doi.org/10.1080/01694243.2026.2658173

in the literature to enhance the adhesive joints' strength, the method of developing mixed bond overlap is gaining popularity for single lap joints. Ramezani et al. [5] investigated the effects of various parameters, such as the ratio of flexible adhesive at the lap end to the total lap length, on the strength of a mixed-bond area lap joint, which was analyzed using the digital image correlation (DIC) technique. They also conducted a numerical analysis to analyze the effect of the length ratio on the strain distribution along the bond line. They reported that the effect of the lap length ratio on the adhesive peel strain increased as the adhesive thickness increased and decreased as the stiffness of the plate increased. Bavi et al. [6] optimized the single and double lap geometry in mixed adhesive bondline using a modified version of bees and genetic algorithms. They identified the application of a yield criterion on the adherend and the geometric constraints on the lap length as constraints for optimization. They reported that the algorithms provided a more accurate approximation of the failure load in mixed adhesive single- and double-lap joints compared to the Volkersen solution. Oz and Ozer [7] investigated the von Mises stress variation in a single-lap joint with a bi-adhesive bond line. They configured the bi-adhesive bond line to have a rigid adhesive in the middle section and ductile adhesives at the edges. Their study involved an analytical approach (Zhao closed-form) and a finite element method. They concluded that an appropriate bond length ratio should be used to achieve high bond strength. Machado et al. [8] investigated the strength of the composite single lap joint with a mixed adhesive bond line under quasi-static and impact loads. The experiment was conducted under low (−30 °C) and high (80 °C) temperatures. They concluded that a mixed bond line improves the performance under both static and impact conditions. The behavior of single lap joints with mono- and bi-adhesive overlap under various loadings is documented in the literature [9–16].

Numerical analyses of single-lap adhesive joints under various loading conditions are quite common in the literature. However, only a few numerical analyses have been reported on lap joints with mixed adhesive bond lines. Pires et al. [17] conducted studies into the tensile strength of a single-lap joint with a biadhesive bond line. In a biadhesive joint, the adhesive at the joint edges is more flexible, while at the center of the lap, it is less ductile. They found that the biadhesive single lap joints gave higher shear strength compared to joints using one adhesive along the complete length of the joint. Carvalho et al. [18] investigated the strength of a single-lap joint manufactured from AW 6082-T651 aluminum adherents. They applied a brittle-ductile combination of adhesives in the overlap area, namely brittle adhesive in the middle and ductile adhesive at the edges. They studied the peel and shear stress variation in the bi-adhesive bond line by numerical analysis using the cohesive zone method. The outcomes revealed that the lap joints with a bi-adhesive bond line showed higher damage tolerance than those made from a single adhesive. Ozer and Oz [19] conducted an investigation on the EDP yield criterion for a single-lap joint model with a hybrid bond line. Nonlinear finite element analyses of single and bi-adhesive joints were performed by using the EDP material model. The results of their investigation showed that when the overlap length ratios are correctly chosen and suitable adhesives are used along the overlap length, the strength of bi-adhesive joints can be increased remarkably compared to that of single adhesive joints.

G.P. Marques et al. [20] investigated the effect of adhesive selection on the strength of single-lap adhesive joints using hybrid (bonded and welded) techniques with different overlap lengths (LO). They compared experimental results with finite element model results. In their finite element analysis, they identified the area where adhesive was applied to the lap joint using the Cohesive Zone Model (CZM). As a result, they stated that single-lap joints with a hybrid bonding region showed strength improvements compared to lap joints containing mono-adhesive. Recent developments have also explored modified Hashin–Puck formulations for improved damage prediction in composite laminates and advanced cohesive zone concepts incorporating graded traction–separation laws for enhanced interface modeling [21–26].

There is restricted literature available to fully explain the mechanical and microstructural properties that influence joint performance in mixed adhesive systems with thermoplastic particle reinforcement. Previous research has not sufficiently addressed the combined effects of thermoplastic reinforcement within mixed adhesive architectures, leaving gaps in understanding their influence on load transfer, damage evolution, and failure behavior. Moreover, this research suggests that it is possible to create single lap joints with a mixed adhesive by using a single adhesive system with thermoplastic reinforcement, which would be an easier and functionally viable option. The present work aims to address these limitations by evaluating the mechanical response, microstructure characteristics of the manufactured adhesive joint, and joint performance analysis. Furthermore, they will advance the development of hybrid adhesive joints and applications in engineering structures.

2. Materials and methods

2.1. Materials and production

This section will describe the materials that comprise the structure of the single-lap joint and describe the fabrication of the lap joint. For the adherends in the single-lap joint, titanium (Ti) and Boron (B)-rich A356 aluminum plate and plain-woven glass reinforced composite laminate were used. The aluminum to be used in the experiments was fabricated by remelting scrap aluminum. Scrap pieces were melted in a 10 kW electrical resistance furnace, and the temperature of the molten metal was measured continuously using a thermocouple. At a temperature of 720 °C, the A356 alloy was melted according to predetermined casting conditions. For grain refinement, titanium (Ti) and boron (B) were added to the melt at a ratio of 0.01% of the total mass. Then the molten alloy was poured into the sand mold. During casting, it is crucial to purify the melt by removing inclusions from it. Therefore, a rotary degassing system was utilized. A graphite lance was plunged into the melt and rotated at a predetermined speed to create a vortex. Nitrogen gas was injected throughout the melt through the special impeller head, and the generated bubbles helped to carry the impurities up toward the top. During this time, the flow rate of nitrogen and impeller rotation speed were maintained at 5 L/min and 300 rpm, respectively. The Reduced Pressure Test (RPT) apparatus was utilized to assess the efficiency of the degassing process. This vacuum solidification technique increases the visibility of entrapped gases and inclusions, thus enabling their assessment. After the solidification of the metal in the mold, the aluminum adherends were taken out and then machined into the required dimensions to assemble the lap joint (Section A in Figure 1).

Composite laminate was manufactured using the VARTM technique. In the composite laminate, glass fiber was used as the reinforcement material, and Araldite LY1564/Aradur epoxy adhesive with an approximate viscosity of 320 MPa·s was used as the matrix material. Furthermore, the reinforcement material and matrix were produced using equivalent volume fraction. In VARTM, sealing tapes were placed around the mold at the start of the VARTM process, while a release film was laid onto the tool surface. Then the dried reinforcement layers were stacked on top of the release film one after another. A flow distribution medium was applied to ensure that the epoxy resin and hardener could proceed uniformly through the structure. The spiral hoses were attached to the ends of the resin inlet line and the vacuum line. Air inside the vacuum bag was sucked away through the hose connected with the vacuum pump, but the mixture of resin and curing agent was simultaneously sucked into the laminate through the spiral resin inlet. This process continued until the epoxy–hardener mixture fully saturated all layers. Once the impregnation process was completed, the layup was placed on top of a heated plate at 100 °C for one hour, allowing the resin to cure. Composite materials were made in eight-layer laminates in an alternating warp and weft orientation. Once cured, 8-layer 2 mm thick composite laminates were cut to the required lap-joint dimensions (Section B in Figure 1).

Araldite 2015 and Araldite Av138M epoxy adhesive manufactured by Huntsman Corporation were mixed with a high-hardness heat-resistant co-polyester thermoplastic (Copes) produced by Schaetti®. The mixing was done using a vacuum-assisted mixing setup. The physical properties of thermoplastic material are available in literature [27]. In general, during adhesive preparation, the addition of hardeners and additives causes air bubbles to form in it. Air bubbles are a common imperfection known to decrease the quality and strength of the bonded joint. To avoid this problem, the entire mixing process was conducted under vacuum conditions. It was ensured that the entrapped air in the adhesive mixture was removed effectively during the process. Vacuum mixing setup components include a vacuum chamber, plastic mixing container, DC motor, mixing blade, potentiometer for speed control, vacuum gauge, filter, valve and vacuum pump. This pump can generate a vacuum with a pressure of 850 mbar. The valve is located between pump and vacuum tank to maintain a constant vacuum. Adhesives are mixed in controlled rotational speed under a vacuum environment, and the rotational speed is precisely set using a potentiometer available in the setup (Section C in Figure 1).

Single-lap joints were manufactured using the 3D printer with a custom mold that was designed especially for the dimensions of the lap joint, so as not to allow any lateral shifting in the axial direction during the curing process of the lap joint. Both fixing pins and a vise were utilized to provide proper alignment (Section D in Figure 1).

2.2. Material characterization

This section will explore how Copes thermoplastic particles incorporated into adhesives affect the mechanical properties of the adhesives, their transition to the polymer phase, and their distribution in adhesives. In the current work, Copes-modified epoxy

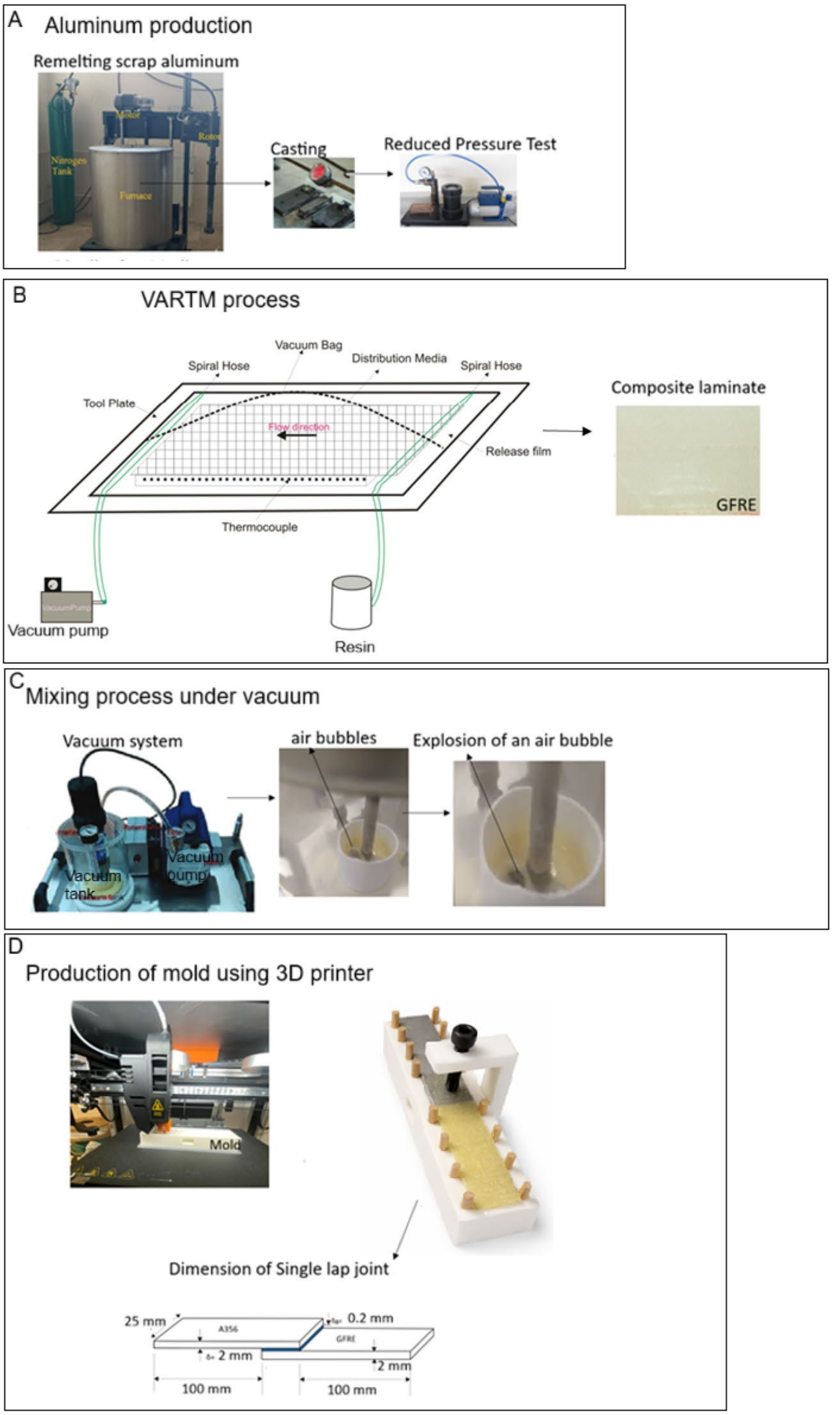

Figure 1. The manufacturing process of the single lap joint.

adhesives were cured at two different temperatures: at the thermoplastic material melting point of 120 °C and at room temperature. Scanning Electron Microscopy (SEM) analyses were conducted during the initial phase of our characterization to study the distribution of Copes particles at RT and after polymerization upon melting at 120 °C, in both Araldite 2015 and Araldite AV138M adhesives. Samples were coated with a gold/palladium (Au/Pd) layer before SEM analysis through a sputter coater, which helped with the electrical conductivity of the surface. The thickness of the coating was between 5 and 10 nm, done in an argon atmosphere of ~0.05–0.1 mbar with a sputtering current of 20–30 mA for 60–90 s. A conductive coating helps charge build-up at the surface with high magnification. This is useful because the probe cannot burn or darken the surface due to the deposition of damaging energy on the surface. Imaging at a magnification of 1,000× was undertaken for assessing interfacial characteristics. SEM images of both adhesives reinforced with COPES are presented at room temperature and 120 °C in Figure 2.

Figure 2 shows that the Copes thermoplastic particles were clearly dispersed within both adhesives at RT. For the adhesive cured at 120 °C, which is considered the melting point of the Copes thermoplastic particles, these particles were seen to melt and polymerize. The bond structure that formed during polymerization also appeared clearly in the SEM image for the Araldite 2015 epoxy adhesive. In the SEM images for both adhesives, thermoplastic particles clearly visible in the RT were seen to melt at 120 °C. It should be noted that thermoset epoxy adhesives usually have a void within their grain boundaries [30]. Those voids also appeared in the SEM analyses carried out as a part of this study.

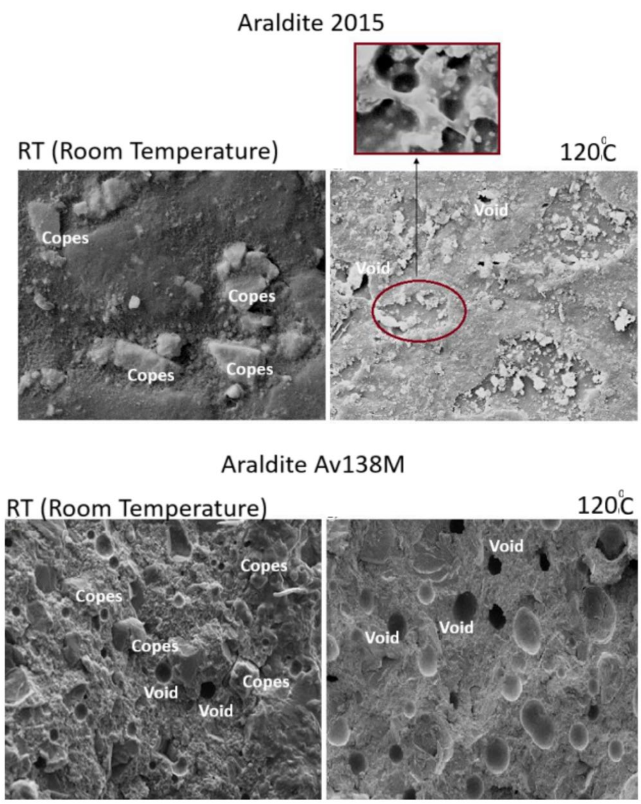

Figure 2. SEM images of both adhesives reinforced with COPES are presented at RT and 120 °C.

This study also focused on the effect of Copes thermoplastic particles on the mechanical properties of epoxy adhesives cured at RT and 120 °C. For this purpose, tensile tests were carried out in an INSTRON 5982 universal testing machine at a loading rate of 1 mm/min. Tests were conducted both at RT and 120 °C by taking advantage of the closed-loop control system of the testing machine. Moreover, with the help of a video extensometer compatible with the testing equipment, it was possible to characterize the linear elastic mechanical properties of the adhesive. Experimental stress- strain curves of both reinforced and unreinforced adhesives tested at RT and 120 °C are illustrated in Figures 3 and 4.

In Figures 3 and 4, it is observed that the stress-strain curve at RT as well as at 120 °C reveals the effect of Copes on the strain and stress of both adhesives. Moreover, the effect of the addition of Copes on the brittle adhesive Av138m epoxy

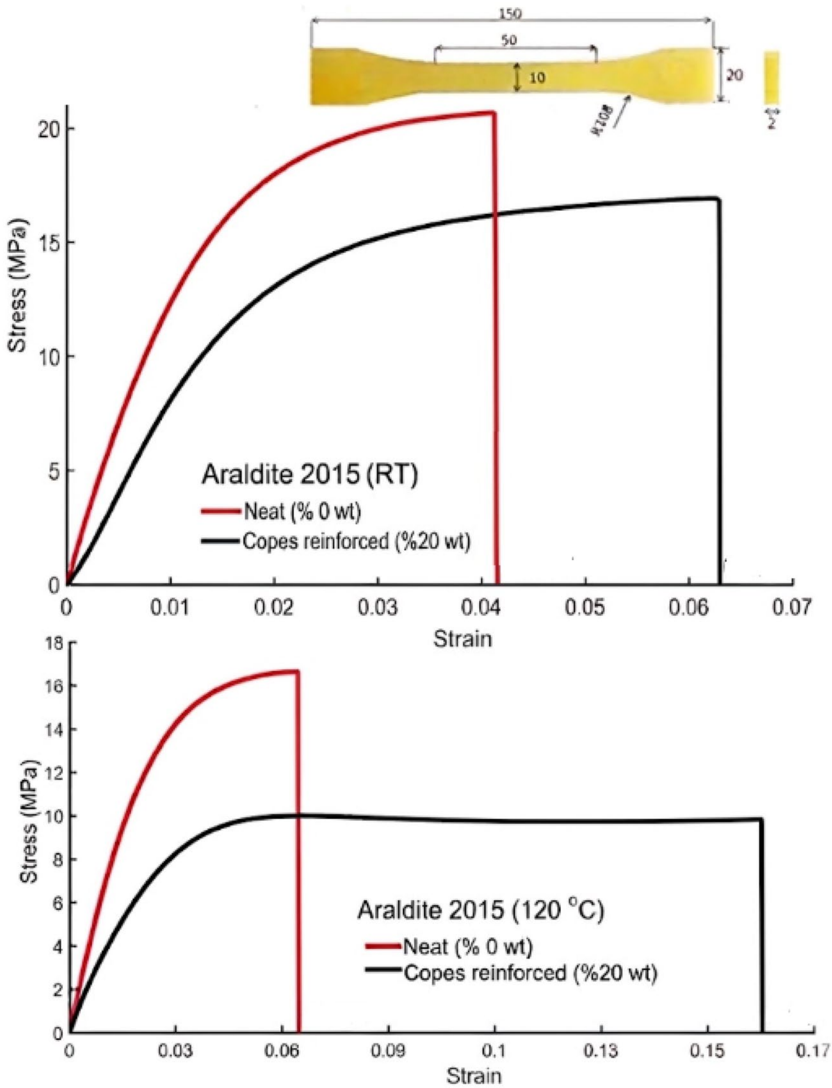

Figure 3. Stress-strain curve for Araldite 2015 adhesive at RT and 120 °C.

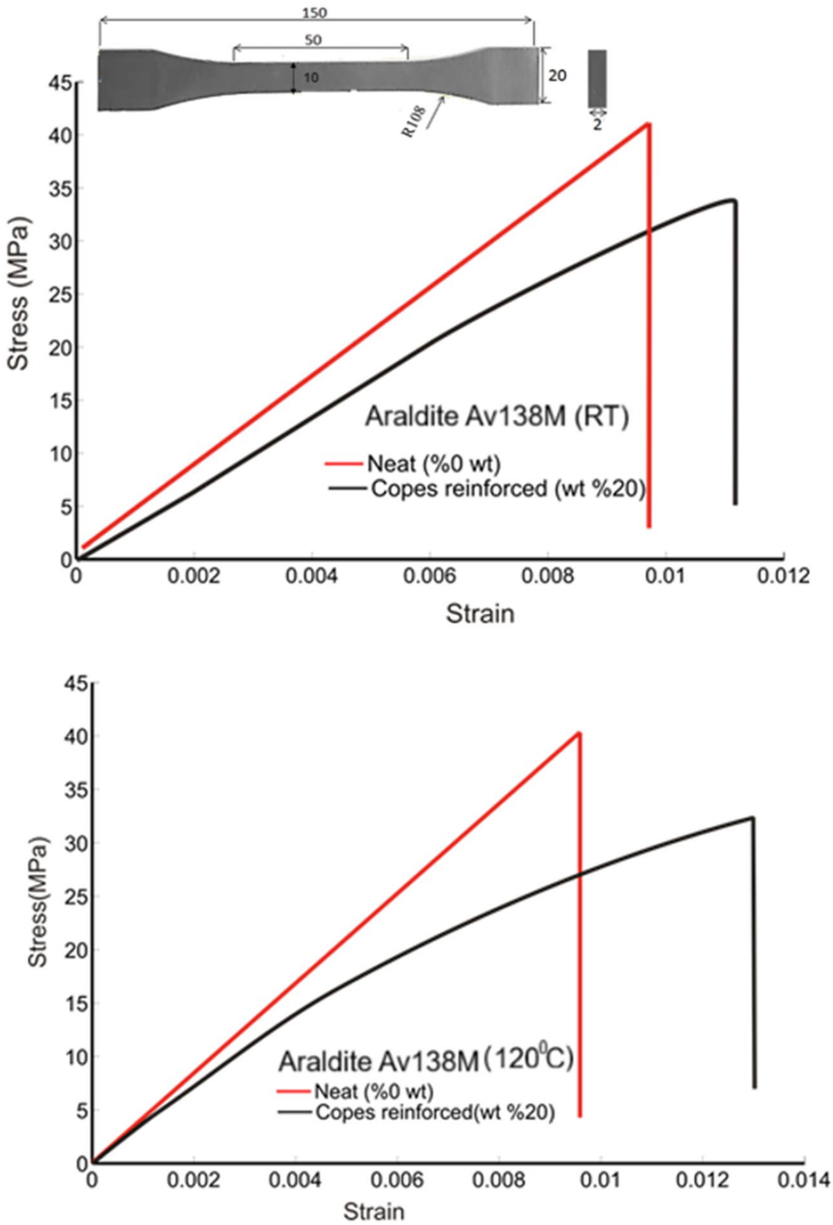

Figure 4. Stress-strain curve for Araldite Av138M adhesive at RT and 120 °C.

adhesive is noticed, as there is a considerable increment in the strain of that adhesive. Thus, it could be concluded that the incorporation of Copes into adhesives causes an increase in the ductility of the adhesives. The mechanical properties derived from the adhesives, as a result of tensile tests conducted at room temperature (RT) and 120 °C, are shown in Tables 1 and 2.

Tables 1 and 2 show that the 20% reinforcement of Copes reduced the tensile strength of the adhesives with an increase in failure strains at both RT and 120 °C.

Table 1. Mechanical properties of the unreinforced/reinforced adhesive at RT [28].

Adhesives	Properties	Unreinforced adhesive	Reinforced adhesive	
	Elasticity modulus (MPa)	1750 ± 35.75	991 ± 44.35	
Araldite 2015	Ultimate tensile strength (MPa)	20.3 ± 2.25	15.5 ± 2.55	
	Failure strain (%)	4.18 ± 0.25	6.45 ± 0.37	
	Elasticity modulus (MPa)	4204.91 ± 72.55	3379.97 ± 48.05	
Araldite Av138M	Ultimate tensile strength (MPa)	41.25 ± 4.15	32.90 ± 3.55	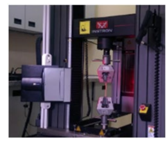
	Failure strain (%)	0.96 ± 0.04	1.15 ± 0.12	

Table 2. Mechanical properties of the unreinforced/reinforced adhesive at 120 °C.

Adhesives	Properties	Unreinforced adhesive	Reinforced adhesive	
	Elasticity modulus (MPa)	1556 ± 40.15	867.72 ± 39.22	
Araldite 2015	Ultimate tensile strength (MPa)	16.27 ± 1.85	10.1 ± 1.45	
	Failure strain (%)	6.11 ± 0.33	16.05 ± 1.17	
	Elasticity modulus (MPa)	4425 ± 45.55	3614.25 ± 32.25	
Araldite Av138M	Ultimate tensile strength (MPa)	40.24 ± 3.05	31.60 ± 2.75	
	Failure strain (%)	0.92 ± 0.025	1.35 ± 0.15	

In addition, it was observed that the modulus of elasticity decreased with the addition of Copes in both adhesives. It should be stated here that different percentages of the Copes were incorporated into the adhesive; however, higher changes were achieved with 20% addition.

In this material characterization study, we conducted a thorough investigation into the distribution of Copes thermoplastic particles within the adhesive, as well as their polymerization behavior at the melting point. Additionally, we assessed the impact of these particles on the mechanical properties of the adhesives. The findings indicate that the adhesives demonstrate compatibility with the Copes thermoplastic particles.

2.3. Mechanical properties of the adherends

The mechanical properties of adherends used for forming the single lap joint were determined using a coupon universal testing machine. Tensile tests were performed at a loading rate of 1 mm/min using a device with a 50-kN load cell and extensometer. The details of the tests performed to assess the mechanical behavior of the materials are available in the authors' previous study [18,19]. The mechanical properties of the adherends are presented in Tables 3 and 4.

3. Experimental study

In the experimental approach, tensile tests of metal composite lap joints at room temperature and 120 °C were performed on an INSTRON 5982 dual-column universal testing machine with a video extensometer. The maximum load capacity of the device is 100 kN, and the load cell accuracy is approximately 0.5%. In all experiments, the loading rate was determined as 1 mm/min. In the experimental approach, metal-composite lap joints were formed using different adhesives. Accordingly, single lap joints were created using neat Araldite 2015 epoxy (*AL-GFRE-2015*), an lap joint was created with Araldite 2015 epoxy adhesive reinforced with 20% copolyester (*AL-GFRE-CO2015*), an lap joint was created using neat Araldite AV138M epoxy (*AL-GFRE-138M*), an lap joint was created with Araldite AV138M epoxy adhesive reinforced with 20% copolyester (*AL-GFRE-CO138M*), an lap joint was created with a mixed overlap region where 138 M brittle adhesive was used in the middle and 2015 ductile adhesive was used at the edges (*AL-GFRE-2015-138M-2015*). A lap joint where 138 M brittle adhesive was used in the middle and 2015 ductile adhesive reinforced with 20% copolyester was used at the edges (*AL-GFRE-CO2015-138M-CO2015*), and finally, a single lap joint was formed with 138-M brittle adhesive in the middle section and 138 M adhesive reinforced with 20% copolyester at the edges (*AL-GFRE-CO138M-138M-CO138M*). The hybrid samples were prepared by considering the effects of both flexible and rigid adhesive lengths in the form of a mixed adhesion region. As a result, relevant studies from the literature were reviewed to evaluate different ratios of flexible adhesive length to rigid adhesive length [31]. The

Table 3. Mechanical properties of the aluminum materials [28].

Properties	A356	A356-TiB
Elasticity modulus (MPa)	69850 ± 2150	71350 ± 1750
Ultimate tensile strength (MPa)	100.5 ± 4.6	118.2 ± 3.15
Yield strength (MPa)	82.75 ± 3.75	88.5 ± 3.15
Failure strain (%)	2.5 ± 0.25	2.75 ± 0.35

Table 4. Mechanical properties of the composite laminate [28,29].

Properties	GFRE
Elasticity modulus (MPa)	35000 ± 1250
Ultimate tensile strength (MPa)	590 ± 30
Poisson ratio	0.3 ± 0.03
Failure strain (%)	2.29 ± 0.18

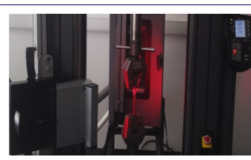

most suitable ratio for these adhesives was identified and applied in the experiments. Additionally, it is noted that silicone tape or fishing line is commonly used in the literature to separate adhesive zones. However, since this study involves experiments conducted at 120 °C, fire-resistant aluminum strip tapes were utilized to ensure high-temperature resistance. Three sets of each single lap joint were created and tested. Samples were prepared in various configurations at different temperatures, following the ASTM D 1002 standard. MATLAB's Moving Average method was used to obtain the average results of the test data. Figure 5 presents the experimental setup, along with an image of a single lap joint featuring a mixed adhesive region.

4. Numerical study

In the numerical study, the single lap joints are created with the dimensions used in the experimental approach. An orthotropic elastic material was utilized for the composıte adherends, while an isotropic elastic material model was assigned to the metallic substrate. In experimental studies, no permanent deformation was observed under any of the conditions examined for both composite laminates and aluminum plates. As a result, plastic behavior was not included in the numerical model, and all components were modeled assuming elastic material properties. Existing literature supports the practice of treating the adherends that constitute lap joints as elastic when investigating their numerical behavior following tensile tests [32]. The orthotropic elastic material model, the global coordinate, and the material coordinate system were used together for modeling the adherends. Three coordinate systems were determined between the nodes and perpendicular to each other. For the orientations in the composite material to be defined correctly to the finite element program, the material coordinate system should be used [33]. Moreover, normal and tangential deformations occur on the adhesive layer under tensile loading. Therefore, the mixed-mode cohesive zone model is applied for modeling the adhesive. Stress expressions using quadratic stress criteria in the mixed-mode cohesive zone model can be defined as [34]

$$\left(\frac{\sigma_I}{\sigma_{um,I}}\right)^2+\left(\frac{\sigma_{II}}{\sigma_{um,II}}\right)^2=1 \quad \text{if } \sigma_I \geq 0$$
$$\sigma_{II}=\sigma_{um,II} \quad \text{if } \sigma_I \leq 0 \tag{1}$$

where $\sigma_{um,I}$ and $\sigma_{um,II}$ are the stresses in the normal and tangential directions, respectively. The deformation values corresponding to the stresses in the cohesive model are as follows [34]:

$$\delta_{om,i}=\frac{\beta_i\delta_{om}}{\sqrt{1+\beta^2{}_{II}}} \tag{2}$$

$$\delta_{um,i}=\frac{\beta_i\delta_{um}}{\sqrt{1+\beta^2{}_{II}}} \tag{3}$$

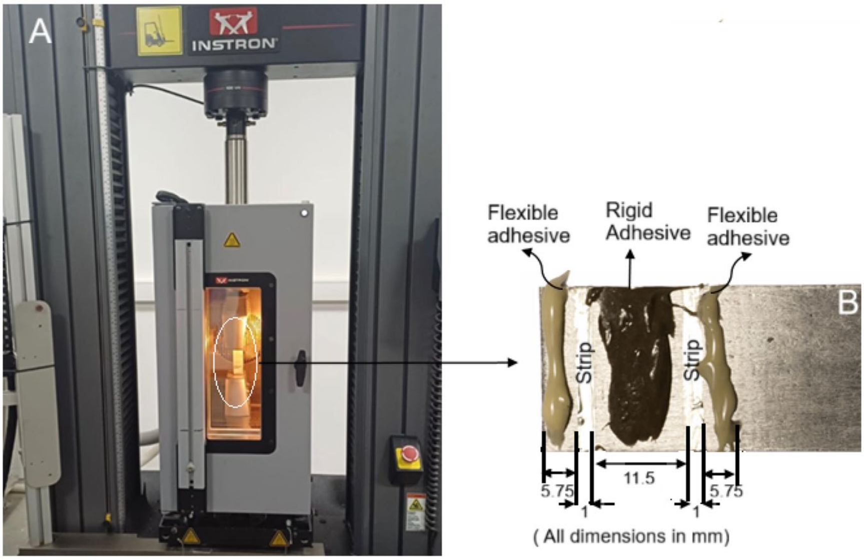

Figure 5. Tensile test device and a single lap joint featuring a mixed adhesive region.

where $\delta_{om,i}$ is the damage onset displacement, $\delta_{um,i}$ is the ultimate failure displacement, and i is the mode number. β_i represents the mode ratio and is shown as follows [34]:

$$\beta_i = \frac{\delta_i}{\delta_I} \tag{4}$$

The cohesive parameters used in the mixed-mode cohesive zone model are indicated in Figure 6. The cohesive parameters of the adhesives have been presented in related studies [35,36]. The stress–strain graphs shown in Figures 3 and 4 were used to determine the cohesive parameters of thermoplastic reinforced adhesives.

4.1. Implementation of the numerical model

A numerical model was developed using the explicit finite element code LS-DYNA. The geometry describing the experimental configuration was modeled. The composite parts were described by using the orthotropic model, whereas the metallic substrates were described using the isotropic elastic model. The adherends in the single-lap joint were meshed using eight-node solid elements, whereas the adhesive layer was meshed using the eight-node mixed-mode interface model (MAT 138), which is available in the LS-DYNA code. For the application of boundary conditions, the single lap joints are constrained in translation along all directions except the coordinate axis on which the load is applied, while the x-axis rotation was prevented indirectly. In simulating the overlap region, contact among the three adhesive layers was defined. A two-way surface-to-surface contact element was applied, whereas the contact nodal

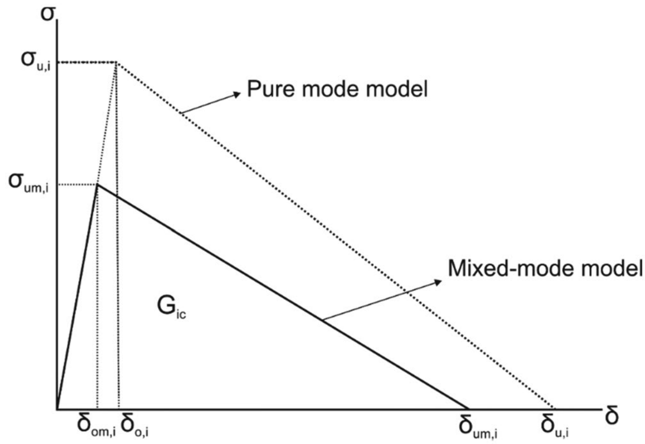

Figure 6. Mixed-mode cohesive zone model [29].

points were defined by using tied nodes to surface contact method. To increase the numerical efficiency of the contact interfaces, the mesh was refined. The refined mesh describes the attempt to increase the numerical efficiency by reducing the penetration errors and by improving the convergence properties [37]. Additionally, the contact between the adhesive and the adherends was described by using eight-node cohesive elements. The loading rate applied to the single-lap joint was utilized through the *prescribed-motion* command. The boundary conditions corresponding to the experimental configuration were applied. In explicit analyses, the numerical description of the termination time has a great influence on the time-dependent simulations. Hence, the termination time was selected appropriately to simulate the experimentally observed deformation and results. In finite element analysis, the effect of temperature during the tensile test simulation can be displayed using the *initial* command within the program. It is important to note that using the *initial* command alone is not sufficient to observe the effect of temperature. The thermal solver located in the control section of the program must be activated. In the present study, the temperature-dependent mechanical behavior of the adhesive was explicitly considered through an experimental approach. Both the neat and copolyester-reinforced adhesive systems were characterized at elevated temperature (120 °C) *via* mechanical testing (Tables 1 and 2). The obtained properties were directly implemented into the numerical model, particularly within the nonlinear cohesive zone modeling framework, where accurate representation of damage initiation and evolution is critically governed by adhesive behavior. To achieve the sensitivity of the mesh and ensure the accuracy of the calculation results, the cohesive layer mesh contains a total of 6090 nodes and 3750 elements. The mesh of the adherends contains 11,934 nodes and 7500 elements, as shown in Figure 7.

5. Results and discussion

This section explains and compares the experimental and numerical results. Initially, the load–displacement graphs obtained from experiments at room temperature and 120°C are shown in Figures 8 and 9.

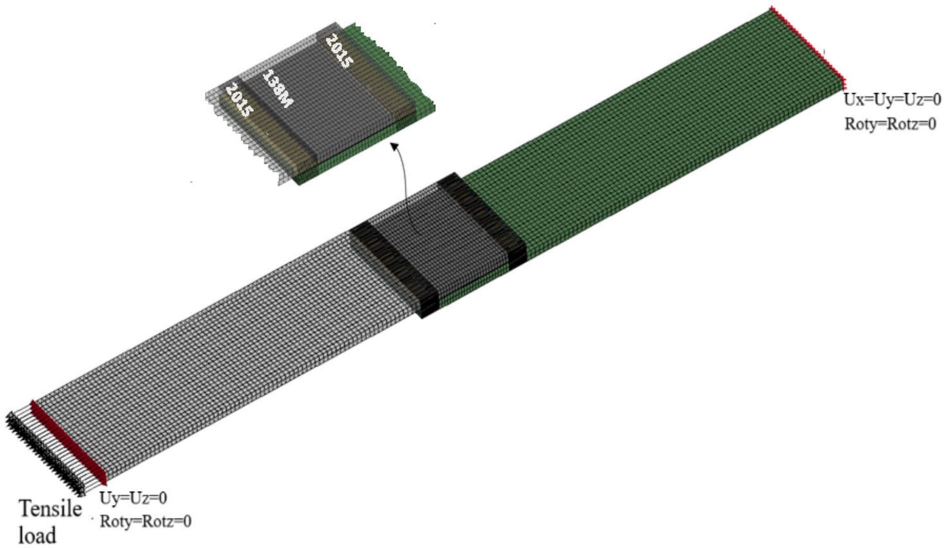

Figure 7. Finite element model of the single lap joint having a mixed overlap region.

As shown in Figures 8 and 9, the strength of single lap joints with a mixed overlap region in two different temperature environments was found to be higher than that of single lap joints with mono-adhesive. However, the addition of reinforcement with Copes resulted in an increase in the values of displacement and a decrease in the values of load in single lap joints with mono-adhesive. In addition, the strength of the single lap joint with a mixed adhesive overlap containing Copes thermoplastic additives was found to be higher than that of the unadded state at both temperature values (see SP5 and SP6 values in Table 5). The reinforcement with Copes resulted in an increase in the ductile behavior of single lap joints and an increase in the amount of energy absorbed by the joints. The strength of single lap joints was reduced when the temperature reached 120 °C. This reduction occurs because epoxy adhesives lose their strength at high temperatures due to factors such as polymer chain degradation, thermal expansion mismatch, and weakening of the interface [38]. Furthermore, it was observed that an increase in the displacement values of all single lap joints occurred due to the melting of the Copes polymer at 120 °C. At this temperature, single lap joints exhibited low energy absorption values. It has been reported that this could be attributed to the facilitation of dislocation movements or the weakening of bonding forces within the adhesive's microstructure [39]. The strength and mechanical properties of a lap joint are affected by the integration and homogeneous distribution of thermoplastic particles within the adhesive. The microscale bonding structures formed during polymerization in Figure 2 were found to hinder crack propagation and increase energy absorption. As a result, a considerable enhancement occurs, particularly in fracture toughness and impact resistance. Moreover, SEM figures indicate that the regular, agglomeration-free distribution of thermoplastic particles minimizes stress concentrations, allowing more balanced load transfer. This plays a role in the creation of cohesive damage in lap joints. To clarify the comments regarding Figures 8 and 9, the maximum load and

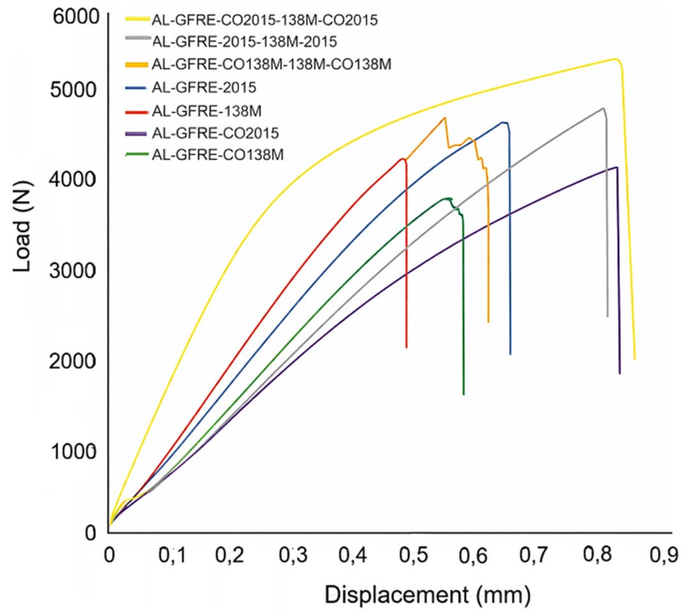

Figure 8. Load–displacement curve at room temperature.

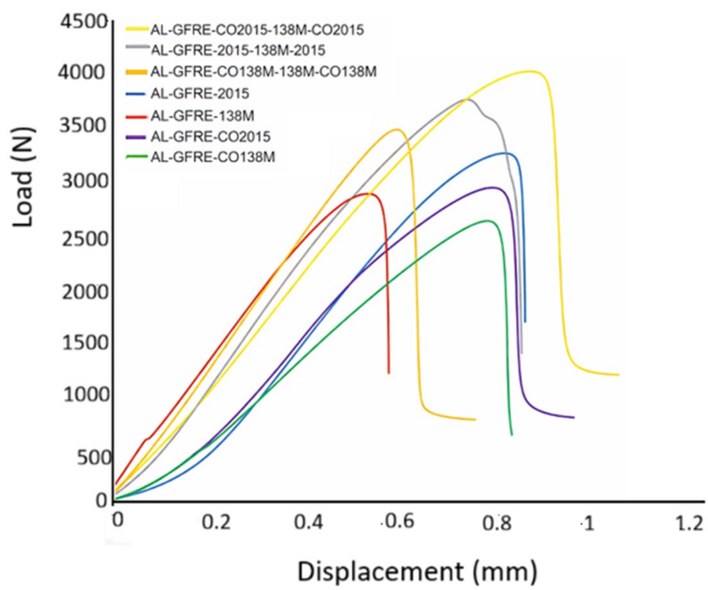

Figure 9. Load–displacement curves at 120 °C.

displacement values at different temperature environments and the absorption energy values formed by the load and displacement curves are presented in Table 5.

Finally, the new finding of the current research is that the strength and absorption energy of a mixed adhesive lap joint consisting of a single adhesive and its thermoplastic reinforced state is better than a lap joint made with the mono-adhesive alone (see SP3 and SP7 values in Table 5). This observation is consistent across

Table 5. Experimental results obtained for all single lap joints from two different temperature environments.

Temperature	Sample	Maximum load (N)	Maximum displacement (mm)	Absorbed energy (Nmm)
	SP1	4851 ± 158	0.66 ± 0.08	1828 ± 99
Room temperature	SP2	4495 ± 183	0.85 ± 0.06	2153 ± 125
	SP3	4423 ± 227	0.49 ± 0.04	1186 ± 112
	SP4	4015 ± 249	0.59 ± 0.08	1257 ± 154
	SP5	5513 ± 198	0.87 ± 0.1	3613 ± 166
	SP6	5264 ± 266	0.82 ± 0.7	2199 ± 189
	SP7	4965 ± 183	0.63 ± 0.9	1623 ± 86
	SP1	3344 ± 225	0.85 ± 0.06	1370 ± 188
	SP2	3062 ± 187	0.95 ± 0.11	1390 ± 201
	SP3	2970 ± 205	0.6 ± 0.05	1028 ± 105
120 °C	SP4	2763 ± 179	0.82 ± 0.07	1126 ± 113
	SP5	4040 ± 255	1.04 ± 0.09	2225 ± 175
	SP6	3810 ± 210	0.84 ± 0.05	1801 ± 190
	SP7	3530 ± 195	0.77 ± 0.06	1328 ± 125

SP1: AL-GFRE-2015, SP2: AL-GFRE-CO2015, SP3: AL-GFRE-138M, SP4: AL-GFRE-CO138M, SP5: AL-GFRE-CO2015-138M-CO2015, SP6: AL-GFRE-2015-138M-2015, SP7: AL-GFRE-CO138M-138M-CO138M ± standard deviation.

both temperature conditions analyzed in the study. Although literature suggests that mixed adhesive overlaps can be formed using at least two different adhesives (one ductile and one brittle), this study demonstrated that a mixed adhesive zone can be created using a single adhesive and thermoplastic reinforcement.

After conducting experiments at two distinct temperature conditions, it was observed that cohesive damage occurred on the surfaces of all adherends in the single lap joints. Cohesive failure is a damage mechanism that occurs when the load is directly transmitted to the adhesive. It can be said that the reliability of the results obtained from lap joints is directly proportional to the cohesive failures obtained. Cohesive failure can occur for various reasons following loading conditions. In particular, for this study, the polymerization and uniform distribution of the thermoplastic particles used contributed to the direct transmission of the load, as observed in SEM analyses and confirmed by the cohesive failures obtained through experimental approaches. Figure 10 presents the images of the cohesive damage recorded at the end of the experiments. However, for the sake of brevity, we have not included images of cohesive damage for all experimental specimens. It is important to note that similar damage patterns were observed across all specimens.

In this study, the results from the experimental approach were compared with those derived from the finite element model. The finite element analysis was carried out under boundary conditions that closely matched those employed in the experimental setup, enabling us to ascertain the maximum load values before failure. The maximum value of the reaction force–displacement curve was used to obtain the maximum load. The ASCII output from LS-DYNA (RCFORC) at a certain time was used. Figure 11 provides a visual comparison of the maximum loads obtained from both the experimental and finite element analyses.

As shown in Figure 11, the highest margin of error between the maximum load values obtained from the experimental approach and the finite element approximation was determined to be approximately 6% for both temperature values. Based on this result, it can be said that the results converged. This validates both the accuracy of the finite element model and the experimental results. Additionally, the experimental

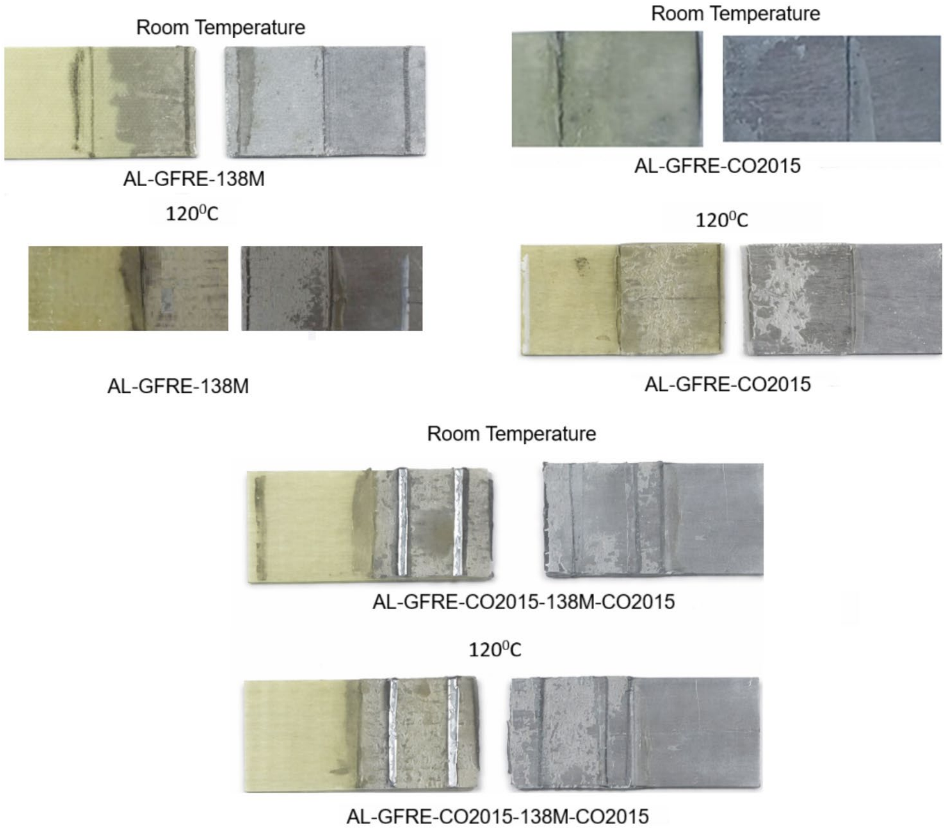

Figure 10. Cohesive damage occurs in single lap joints under varying temperatures.

and finite element damage view of the single lap joint before it reaches complete failure was illustrated in Figure 11(c). In the experimental case, the crack propagation in the overlap region of the single lap joint and the bending occurring in the adherends of the lap joint were very similar to those observed in the finite element model. The main reason is that the adhesive was modeled using a non-linear cohesive element in the finite element model. At this point, the authors emphasize that the contact between the adhesive and the adherend in the single-lap joint should be established absolutely with a cohesive element. In some studies, this contact has been established *via* a contact element. However, the contact element prevents observation of crack propagation and adherend bending since it causes the adherend and adhesive to behave as a whole. This creates a significant difference between the damage obtained in the experimental approach and the damage obtained from the finite element analysis.

In finite element analysis, the shear stresses acting on the adhesive element were analyzed separately for all single lap joints at two different temperatures. The graphs of shear stresses are presented in Figure 12.

As shown in Figure 12, the highest shear stress was obtained from the single lap joints that had a mixed adhesive line for both different temperatures. However, similar to the maximum load behavior, a decrease in maximum shear stresses occurs with the addition of Copes thermoplastic material. When the shear stress behavior

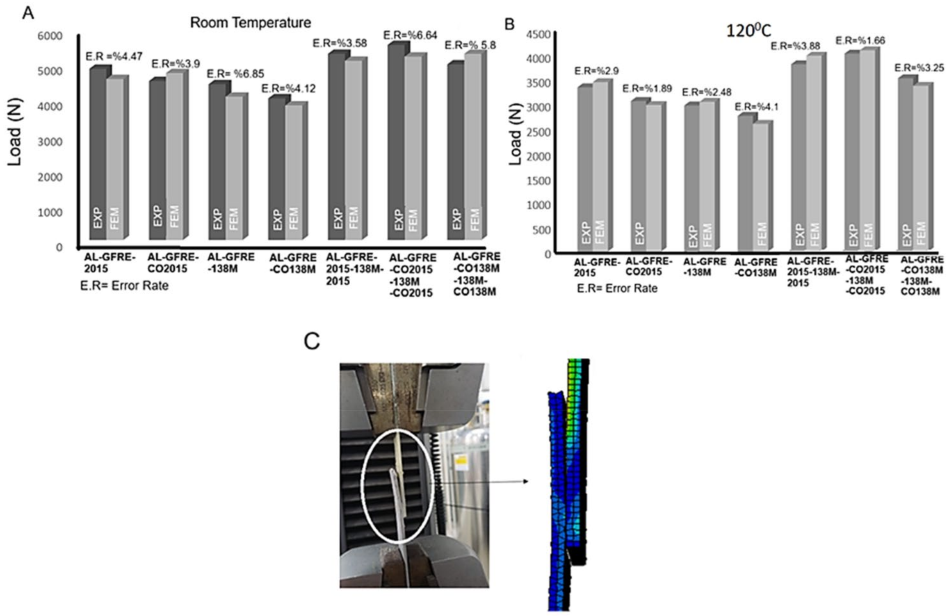

Figure 11. The comparison of the results: (a) room temperature, (b) 120 °C, and (c) comparison of the deformation.

of lap joints created using mono-adhesive was examined, it was observed that the maximum stresses were at the extreme points at the tip of the overlap region and then decreased. In single lap joints using a mixed adhesive region, the maximum shear stress was observed as a peak in the area of the overlap length where the adhesive exhibits ductility. In contrast, the regions with brittle adhesive remained at lower stresses. For lap joints with a mixed adhesive region, the maximum shear stress did not occur at the ends of the overlap length, which differs from the behavior seen in mono-adhesive cases. Similar behaviors were obtained for the mono and mixed adhesive cases of lap joints at 120 °C. However, the shear stress values obtained at 120 °C were lower than those obtained at room temperature. This is due to polymer chain degradation and weakening of the interface. Additionally, examining the shear stress distribution along the mixed adhesion line reveals that the load is distributed more uniformly across the adhesion line than concentrated only at the ends. Distributing the stress over a wider area directly increases the overall load-carrying capacity of the joint. Furthermore, in a mixed-bonding line, stress concentration at the ends of the lap joint is dampened by plastic deformation. This ensures that damage begins as a controlled deformation rather than immediate deboning. Finally, it should be noted that the shear stress behavior of the lap joints has been determined in accordance with the literature [19].

The potential influence of hourglass deformation was carefully considered in the numerical analyses. Reduced integration elements were employed together with appropriate hourglass control to prevent non-physical deformation modes. The reliability of the results was verified by monitoring the ratio of hourglass energy to internal energy, which remained below the commonly accepted threshold throughout the simulations.

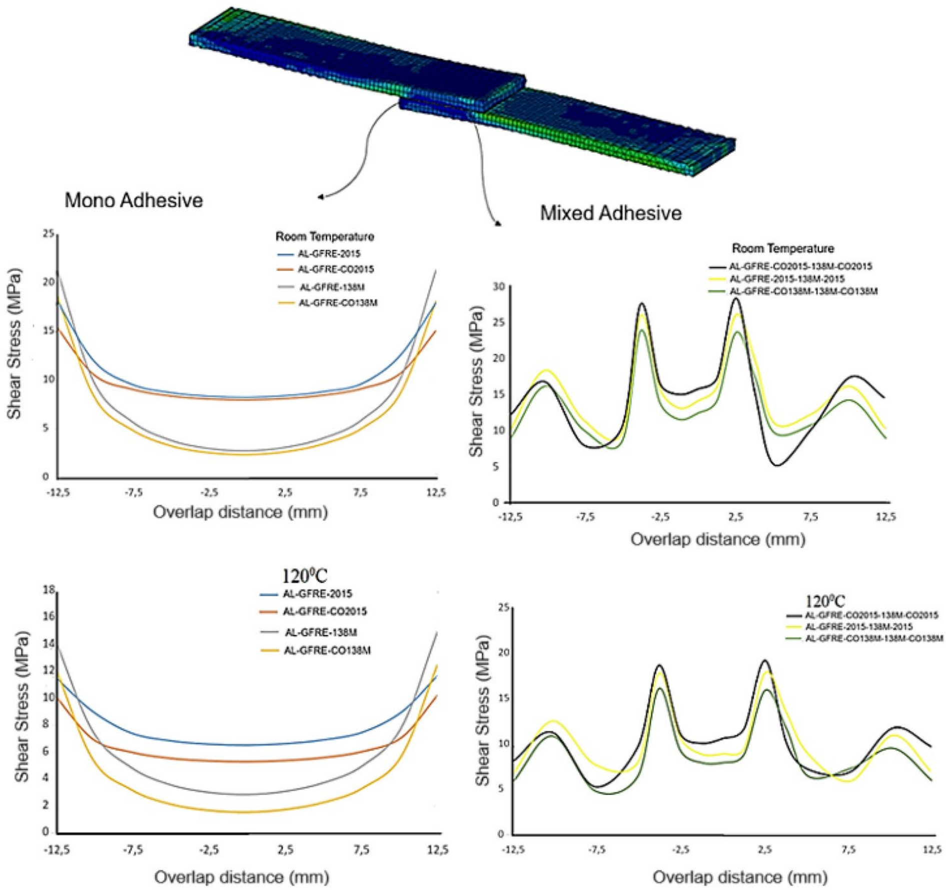

Figure 12. The shear stresses acting on the adhesive element at two different temperatures.

6. Conclusion

This study primarily examines the strength of a single lap joint having a mixed adhesive overlap region consisting of a single adhesive and its thermoplastic reinforced state under varying temperatures. The primary contribution of this study is to demonstrate that a mixed adhesive configuration made of a single adhesive and thermoplastic reinforcement performs better mechanically than a conventional mono-adhesive joint. Past studies often report mixed adhesive systems obtained by combining two separate adhesives, which are usually one ductile and one brittle. However, the present work illustrates that similar performance can be achieved by reinforcing one adhesive with a thermoplastic phase. The quantitative findings supporting the results of this study are listed below.

- At room temperature, the maximum load capacity of a single-lap joint made with Mono 2015 epoxy adhesive is 8% higher than that of a lap joint reinforced with copolyester. In comparison, a lap joint utilizing Mono 138M adhesive exhibited a 9% incline in load capacity, rather than that of a lap joint reinforced with copolyester. Furthermore, the incorporation of copolyester reinforcement provides a significant increase in absorbed energy, with the 2015 epoxy adhesive joint showing an 18% enhancement, while the 138M adhesive joint achieved a 6% increase. Moreover, the lap joint with the mixed adhesion line produced with the 2015 epoxy adhesive and copolyester reinforcement recorded the highest load capacity of all lap joints tested. It was observed that this joint had a load capacity that was 5% greater than that of lap joints with mixed adhesion lines made with mono 2015 adhesive. Also, it was 10% higher than those made with copolyester-reinforced 138M adhesive.

- At 120 ^{0}C, the maximum load capacity of a single-lap joint using Mono 2015 epoxy adhesive exceeds that of a lap joint reinforced with copolyester by 9%. In contrast, a lap joint employing Mono 138M adhesive showed a 7% increase in load capacity, compared to a lap joint supported by copolyester. Moreover, the addition of copolyester reinforcement results in a rise in absorbed energy, with the 2015 epoxy adhesive bond exhibiting an 2% improvement, while the 138M adhesive bond reached a 10% boost. Additionally, the lap joint featuring the mixed adhesion line created with the 2015 epoxy adhesive and copolyester reinforcement exhibited the greatest load capacity among all tested lap joints. This joint demonstrated a load capacity that exceeded lap joints with mixed adhesion lines created with mono 2015 adhesive by 6%. Additionally, it was 14% greater than those produced with copolyester-reinforced 138M adhesive.
- In the numerical analysis results, the highest shear stress among all lap joints was obtained in the lap joint with a mixed adhesive line incorporating copolyester-reinforced 2015 epoxy adhesive. At room temperature, there was a 38% difference between the closest value, while at 120 °C, the difference is approximately 30%. Furthermore, at room temperature, the highest difference in maximum loads obtained from experimental and numerical analysis was from the AL-GFRE-CO2015-138M-CO2015 with 8.5%, while the lowest difference was obtained from the AL-GFRE-CO138M with 2.7%. At 120 °C, the highest difference was obtained from the AL-GFRE-2015with 7.9%, and the lowest difference was obtained from the AL-GFRE-138M with 1.88%.
- Consequently, it can be said that the improved performance of a thermoplastic-reinforced epoxy system indicates good potential for aerospace, marine, and automotive applications in bonded joints under thermal and mechanical loading. In particular, for the aerospace applications, such adhesion systems display lightweight and high thermal resistance, which enhances joint durability and structural integrity under service conditions.

Author contributions

CRediT: **Engin Erbayrak**: Conceptualization, Data curation, Investigation, Methodology, Writing – original draft, Writing – review & editing; **Beril Eker**: Investigation, Visualization, Writing – original draft, Writing – review & editing; **Murat Colak**: Investigation, Methodology, Visualization, Writing – original draft, Writing – review & editing.

Disclosure statement

The authors declared that there is no potential competing interest for this study.

ORCID

Engin Erbayrak http://orcid.org/0000-0002-0648-8823
Beril Eker http://orcid.org/0000-0002-4185-4470
Murat Colak http://orcid.org/0000-0002-8255-5987

References

[1] Wei Y, Jin X, Luo Q, et al. Adhesively bonded joints – a review on design, manufacturing, experiments, modeling and challenges. Compos B. 2024;276:111225. doi: 10.1016/j.compositesb.2024.111225.

[2] Borges CSP, Safar AA, Tsokanas P, et al. From fundamental concepts to recent developments in the adhesive bonding technology: a general view. Discover Mech Eng. 2023;2(8):1–32. doi: 10.1007/s44245-023-00014-7.

[3] Maggiore S, Banea MD, Stagnaro P, et al. A review of structural adhesive joints in hybrid joining processes. Polymers (Basel). 2021;13(22):3961. doi: 10.3390/polym13223961.

[4] Lamberti M, Pantel AM, Lebon F. Mechanical performance of adhesive connections in structural applications. Materials (Basel). 2023;16(22):7066. doi: 10.3390/ma16227066.

[5] Ramezani F, Ayatollahi MR, Akhavan-Safar A, et al. A comprehensive experimental study on bi-adhesive single lap joints using DIC technique. Int J Adhes Adhes. 2020;102:102674. doi: 10.1016/j.ijadhadh.2020.102674.

[6] Bavi O, Bavi N, Shishesaz M. Geometrical optimization of the overlap in mixed adhesive lap joints. J Adhes. 2013;89(12):948–972. doi: 10.1080/00218464.2013.782813.

[7] Öz Ö, Özer H. On the von Mises elastic stress evaluations in the bi-adhesive single-lap joint: a numerical and analytical study. J Adhes Sci Technol. 2014;28(21):2133–2153. doi: 10.1080/01694243.2014.948110.

[8] Machado JJM, Marques EAS, da Silva LFM. Influence of low and high temperature on mixed adhesive joints under quasi-static and impact conditions. Compos Struct. 2018;194:68–79. doi: 10.1016/j.compstruct.2018.03.093.

[9] Kumar S, Pandey PC. Behaviour of bi-adhesive joints. J Adhes Sci Technol. 2010;24(7):1251–1281. doi: 10.1163/016942409X12561252291982.

[10] Marques EAS, da Silva LFM, Flaviani M. Testing and simulation of mixed adhesive joints for aerospace applications. Compos B. 2015;74:123–130. doi: 10.1016/j.compositesb.2015.01.005.

[11] Breto R, Chiminelli A, Lizaranzu M, et al. Study of the singular term in mixed adhesive joints. Int J Adhes Adhes. 2017;76:11–16. doi: 10.1016/j.ijadhadh.2017.02.002.

[12] Yousefsani SA, Tahani M. Relief of edge effects in bi-adhesive composite joints. Compos B. 2017;108:153–163. doi: 10.1016/j.compositesb.2016.09.099.

[13] Sonia S, Mostapha T, Hamza BY. An investigation of in-plane dynamic behavior of adhesively-bonded composite joints under dynamic compression at high strain rate. Compos Struct. 2018;191:168–179. doi: 10.1016/j.compstruct.2018.02.057.

[14] Sonia S, Mostapha T, Hamza BY. Thermomechanical behavior of adhesively bonded joints under out-of-plane dynamic compression loading at high strain rate. J Compos Mater. 2018;52(30):4171–4184. doi: 10.1177/0021998318777048.

[15] Sassi S, Tarfaoui M, Benyahia H. Experimental study of the out-of-plane dynamic behaviour of adhesively bonded composite joints using split Hopkinson pressure bars. J Compos Mater. 2018;52(21):2875–2885. doi: 10.1177/0021998318758368.

[16] Mostapha T, Sonia S, Oumnia L, et al. Strain rate effects on the thermomechanical behavior of glass/polyester composite joints. Polym Compos. 2022;43:36–51. doi: 10.1002/pc.26355.

[17] Pires I, Quintino L, Miranda RM. Numerical simulation of mono- and bi-adhesive aluminium lap joints. J Adhes Sci Technol. 2006;20(1):19–36. doi: 10.1163/156856106775212387.
[18] Carvalho DFT, Campilho RDSG, Vargas AS, et al. Parametric cohesive zone analysis of bi adhesive single step joints. SN Appl Sci. 2023;5(12):377. doi: 10.1007/s42452-023-05586-3.
[19] Özer H, Öz Ö. The use of the exponential Drucker-Prager material model for defining the failure loads of the mono and bi-adhesive joints. Int J Adhes Adhes. 2017;76:17–29. doi: 10.1016/j.ijadhadh.2017.02.005.
[20] Marques GP, Campilho RDSG, da Silva FJG, et al. Adhesive selection for hybrid spot-welded/bonded single-lap joints: experimentation and numerical analysis. Compos B. 2016;84:248–257. doi: 10.1016/j.compositesb.2015.09.002.
[21] Zouggar K, Guerraiche D, Rabouh M, et al. Numerical damage assessment in T700/epoxy composite laminate under low and high velocity impacts using a modified Hashin-Puck criterion. Compos Struct. 2025;372:119578. doi: 10.1016/j.compstruct.2025.119578.
[22] Harmel MW, Zouggar K, Jalalvand M, et al. Numerical damage analysis using FGA-USDFLD based on functionally graded cohesive zone modeling concept for bonded composite patch repairs. Int J Adhes Adhes. 2025;143:104137. doi: 10.1016/j.ijadhadh.2025.104137.
[23] Aminallah S, Madani K, Benyettou M, et al. Numerical analysis of composite patch repairs on damaged plates with optimized geometric modifications for improved fracture strength. Mech Adv Mater Struct. 2025:1–20. doi: 10.1080/15376494.2025.2474212.
[24] Harmel MW, Kouider M, Benyettou M, et al. Effect of patch geometry on the structural performance of damaged plates in bonded patch repairs techniques using a combination of XFEM and CZM techniques. Mech Adv Mater Struct. 2025:1–17. doi: 10.1080/15376494.2025.2507193.
[25] Mostapha T. Prediction of the strength of the adhesively bonded joints by the finite elements method. Appl Mech and Mater. 2011;62:125–134. doi: 10.4028/www.scientific.net/amm.62.125.
[26] Mostapha T, Lotfi H, Sabrine K, et al. Examination of the delamination of a stitched laminated composite with experimental and numerical analysis using mode I interlaminar. Arab J Sci Eng. 2020;45:5873–5882. doi: 10.1007/s13369-020-04599-z.
[27] Copolyester materials (Copes). Schaetti, high performance thermoplastic copolyester; 2012. http://www.schaetti.com/fileadmin/content/pdf/markette_productute/4_Construction.
[28] Erbayrak E, Colak M, Noberi C. Low-velocity impact analysis of metal-composite joints with grain-refined A356 and reinforced epoxy adhesive using six node pentahedron cohesive elements. J Adhes. 2026;102(4):275–299. doi: 10.1080/00218464.2025.2531241.
[29] Erbayrak E, Gumus BE, Yuncuoglu EU. Experimental study of adhesively bonded joints with dissimilar composite laminates under different loading rates and ambient temperatures. J Braz Soc Mech Sci Eng. 2023;45(5):260. doi: 10.1007/s40430-023-04195-w.
[30] Rojek J, Breite C, Swolfs Y, et al. Void growth measurement and modelling in a thermosetting epoxy resin using SEM and tomography techniques. Continuum Mech Thermodyn. 2020;32(2):471–488. doi: 10.1007/s00161-020-00865-5.
[31] Öz Ö, Özer H. An experimental investigation on the failure loads of the mono and bi-adhesive joints. J Adhes Sci Technol. 2017;31(19-20):2251–2270. doi: 10.1080/01694243.2016.1264661.
[32] Khalili SMR, Khalili S, Pirouzhashemi MR, et al. Numerical study of lap joints with composite adhesives and composite adherends subjected to in-plane and transverse loads. Int J Adhes Adhes. 2008;28(8):411–418. doi: 10.1016/j.ijadhadh.2008.04.010.
[33] Livermore Software Technology. LSDYA user manuals. Vol. II; 2014. https://ftp.lstc.com/.
[34] Silva LFM, Rodrigues TNSS, Figueiredo MAV, et al. Effect of adhesive type and thickness on the lap shear strength. J Adhes. 2006;82:1091–1115. doi: 10.1080/00218460600948511.

[35] Campilho RDSG, Fernandes TAB. Comparative evaluation of single-lap joints bonded with different adhesives by cohesive zone modelling. Proc Eng. 2015;114:102–109. doi: 10.1016/j.proeng.2015.08.047.
[36] Özer H, Erbayrak E. The effects of curing temperature on fracture energy and cohesive parameters for the adhesive Araldite 2015. J Adhes Sci Technol. 2018;32(12):1287–1312. doi: 10.1080/01694243.2017.1410080.
[37] Zimmerman BK, Ateshian GA. A surface-to-surface finite element algorithm for large deformation frictional contact in FEBIO. J Biomech Eng. 2018;140(8):0810131–08101315. doi: 10.1115/1.4040497.
[38] Liu H, Fan Y, Peng H. Effect of full temperature field environment on bonding strength of aluminum alloy. Cryst. 2021;11(6):657. doi: 10.3390/cryst11060657.
[39] Wu A, Zhang Z, Yu J, et al. Effect of different temperature on the fracture toughness and fracture behavior of Mg-9.46Gd-3.96Y-2.34Zn-0.42Zr alloy cylindrical component for aerospace applications. J Alloys Compd. 2025;1019:179311. doi: 10.1016/j.jallcom.2025.179311.